Surface-structure dependence of water-related adsorbates on platinum

Badan, C.

Chapter 7

Step-Type Selective Oxidation of Pt Surfaces

7.1 Abstract

Herein, we report on a combined TPD and STM study of O_2 adsorption and dissociation on various Pt surfaces with widely varying (111) terrace widths. Our quantitative TPD results show that (110) stepped surfaces adsorb considerably more oxygen at 100 K, regardless of terrace width, than either (100) stepped surfaces or planar Pt(111). These results suggest that O_2 dissociates on the (110) stepped surfaces at 100 K, well lower than required for temperature-induced dissociation on (111) planes. The amount of oxygen desorbing from recombinative desorption of adsorbed oxygen atoms is also greater on (110) stepped surfaces. In addition, the partitioning of adsorbed oxygen between molecular and dissociative states depends on the step geometry; (110) stepped surfaces show an uptake plateau indicative of a threshold surface concentration for low-temperature dissociation, whereas (100) stepped surfaces do not. Scanning tunneling microscope (STM) images for various O coverages and surface deposition temperatures confirm low temperature dissociation on a (110) stepped surface. The STM

images also show that terrace width is not a factor in the lowered dissociation barriers for O_2 on (110) stepped surfaces.

Based on: Badan, C.; Farber R. G.; Heyrich, Y.; Koper, M. T. M.; Killelea, D. R.; Juurlink, J. Phys. Chem. C, 2016, DOI: 10.1021/acs.jpcc.6b05482

7.2 Introduction

The interaction of oxygen with Pt and other late transition metal surfaces is crucial for many applications of heterogeneous oxidation catalysis such as fuel processing and remediation of exhaust gases[1–4]. In actual industrial catalytic systems, the degree of surface oxidation is key to the catalytic reactivity and behavior. Therefore, numerous experimental and theoretical studies have been conducted to determine the nature of this strong oxidation dependence. Thus far, well defined, low defect surfaces, such as Pt(111) and Pt(100), have revealed much about how O_2 adsorbs and dissociates on Pt surfaces and how the Pt surface is altered upon oxidation[1, 2, 5–7].

O_2 dissociates on Pt(111) to form adsorbed oxygen (O_{ad}), and prolonged O_2 exposures will saturate the surface with an adsorbed oxygen coverage ($\theta_{O_{ad}}$) of 0.25 monolayers (ML) in a (2x2)-O adsorbate layer. Formation of O_{ad} on Pt(111) is a precursor-mediated process where O_2 first sticks to the surface as molecularly chemisorbed O_2 ($O_{2,ad}$). The temperature of the surface (T_s) determines the lifetime and coverage of $O_{2,ad}$ ($\theta_{O_{2,ad}}$); dissociation into O_{ad} is in competition with molecular desorption to O_2 (g). Both processes are thermally activated, but the barrier to desorption is typically lower than dissociation. This results in a surface temperature effect where elevated T_s provide the energy needed for dissociation, but shorten the precursor residence time. If the T_s is too low, there is insufficient thermal energy to dissociate O_2, resulting in stable $O_{2,ad}$. When the surface is warmed, $O_{2,ad}$ is then able to dissociate, but in competition with desorption[1, 8, 9]. $O_{2,ad}$ has also been identified on planar and stepped Pt surfaces using scanning tunneling microscopy (STM)[10], temperature programmed desorption (TPD)[11], and electron-energy-loss spectroscopy (EELS)[12]. On Pt(111), recombinative desorption of dissociated O atoms occurs between 500 K and 850 K in a TPD experiment[11, 13–21]. O_2 exposure at elevated temperatures (400 - 600 K) results in excess of 0.25 ML O, the maximum coverage for oxygen adsorption on Pt(111). Additionally, surface oxidation at coverages greater than 0.25 ML has been observed when using oxygen sources other than O_2[6, 7, 13, 16, 17, 22] such as atomic oxygen[17], electron bombardment of an O_2 covered surface[15], or using NO_2[23] or O_3[24]. The reaction probability is coverage dependent; specifically at low coverages, the dissociation of O_2 on Pt surfaces is enhanced by the presence of O_{ad}[18, 23].

On the more corrugated Pt(110) surface, O_2 dissociation also exhibits a similar temperature dependence. Only $O_{2,ad}$ forms below 180 K, but O_2 can dissociate to O_{ad} at higher temperatures[25]. The saturation coverage of O_{ad} on Pt(110) is 0.25 ML, forming a (2x1) O adlayer, that is the most stable structure for a wide range of conditions[26]. Extended exposures to either atomic oxygen (AO) or high

pressure O_2 exposures lead to higher coverage surface structures, whose stability is strongly temperature dependent[27, 28].

It is well known that steps and other defect sites increases the total reactivity of the surface, particularly for molecularly adsorbed species[1, 29] such as chemisorbed O_2. Theoretical calculations and experimental studies attribute the observed increase in reactivity to the local lowering of the dissociation barriers in close proximity to the step sites[30, 31] as well as to changes in the d-band local density of states of the Fermi energy at kinks on the stepped surface[1]. While it is known that steps and kinks are an essential component for dissociation on metal surfaces, it is unknown whether dissociation mechanisms are enhanced by particular step geometries.

In this study, we investigated the extent to which step geometry influences oxygen dissociation on Pt surfaces. We have used Pt[n(111)x(100)] and Pt[n(111)x(110)] surfaces with n = 3 and 4, respectively. These highly corrugated surfaces have step densities similar to those found on nanoparticles. TPD experiments on several different Pt crystal surfaces were performed in a single UHV chamber with identical thermocouple connections and measurement conditions allowing for direct comparison of the obtained data. As a complement to high resolution TPD data, scanning tunneling microscopy (STM) was used to study the temperature and coverage dependence of O_2 dissociation on Pt(553), which can be further used to explain the dissociation behavior at (110) step types.

7.3 Experimental Section

The equipment and detailed procedures used for angle-resolved TPD experiments at Leiden University have been described elsewhere [18, 32]. Briefly, we use a home-built UHV system with a base pressure of 5×10^{-11} mbar. The chamber is equipped with a differentially pumped quadrupole mass spectrometer (QMS, Baltzers QMA400) that only detects desorption from the polished side of our disk-shaped Pt single crystals. The canister's volume is ∼1.5 L, most of which is occupied by the QMS itself. It is pumped by a 240 L/s turbomolecular pump positioned along the QMS rods, ensuring high pumping speed in the entire volume. In this study, we have used five samples with different surface orientations, most of which were cut from a Pt single crystal boule (Surface Preparation Laboratory, Zaandam, The Netherlands). They are all 10 mm diameter and 1-2 mm thick, have a purity better than 5N, and are aligned with an orientation better than 0.1° from the indicated surface. We cleaned the polished side of our crystals under UHV conditions by repetitive sputtering-annealing cycles. Additionally, all samples were heated at 1200 K for 5 min after each TPD experiment. The samples were

heated radiatively and/or by electron bombardment using a filament (Osram, 250 W) positioned ~ 2 mm behind the crystal. Liquid N_2 was used for cooling during surface preparation and subsequent experiments. The surface temperature, T_s, was measured using K-type thermocouples; each sample has a permanently affixed thermocouple laser welded to its top edge. We have used low energy electron defraction (LEED) (VG RVL 900) to check the surface order and have shown the relevant LEED patterns elsewhere [18, 19, 32]. The calculated spot-row spacing to spot-splitting ratios of these surfaces correspond well to literature values[33]. The LEED patterns confirm long-range order with the expected average terrace width for each of the Pt surfaces. We have also performed a beam energy analysis of the (0,0) spot-splitting of each of the Pt surfaces to confirm that steps are of mono-atomic height [34].

Oxygen (Messer, 5.0) was dosed directly onto the polished surface of the single crystals between 95 K and 100 K using a leak valve with a 6 mm diameter tube attached inside the UHV chamber. We dosed at a fixed distance between sample and the end of this tube. This ensured localized, highly reproducible, O_2 deposition for all five single crystal samples used in this study. During dosing, all filaments in the UHV chamber were switched off. The pressure was monitored by a cold cathode gauge. The heating rate for all subsequent TPD experiments was 1.0 K s^{-1}. To allow for quantitative comparison of TPD spectra obtained from different crystals, the assembly holding our samples contains an isolated copper stud that protrudes from the polished surface just above the crystal. We positioned the samples with high accuracy relative to the 5 mm diameter orifice in the differentially pumped QMS's housing by retracting the sample a fixed distance after the copper wire made electrical contact with the housing. Coverages were obtained from TPD experiments by integrating the QMS signal. The integrated O_2 TPD signal between 500 and 900 K from Pt(111) with saturation coverage of 0.25 ML was used as a reference[11, 14, 15, 35, 36]. Additional details regarding the experimental apparatus, O uptake on Pt surfaces, and calibration of the TPD data are provided in the Supporting Information.

Scanning tunneling microscopy (STM) experiments were performed at Loyola University. Equipment and procedures have been described previously in detail [37]. Briefly, the Pt(553) surface was cleaned following published procedures[20]. Surface cleanliness was confirmed via Auger electron spectroscopy and a sharp LEED pattern[19]. The cleaned Pt(553) surface was dosed at either $T_s = 100$ K or 400 K by backfilling the chamber with O_2. The exposure was verified with a QMS monitoring the O_2 partial pressure. After O_2 exposure, the crystal was cooled to around 90 K, inserted into the STM, and then further cooled to 30 K for imaging. Oxygen coverage was measured via TPD, and agreed well with the

TPD measurements taken in Leiden, as reported in a previous publication[38]. TPDs taken after imaging showed neither any decrease in O_2 desorption nor the accumulation of background gases on the sample. All STM images were obtained with Pt/Ir tips in constant-current scanning mode.

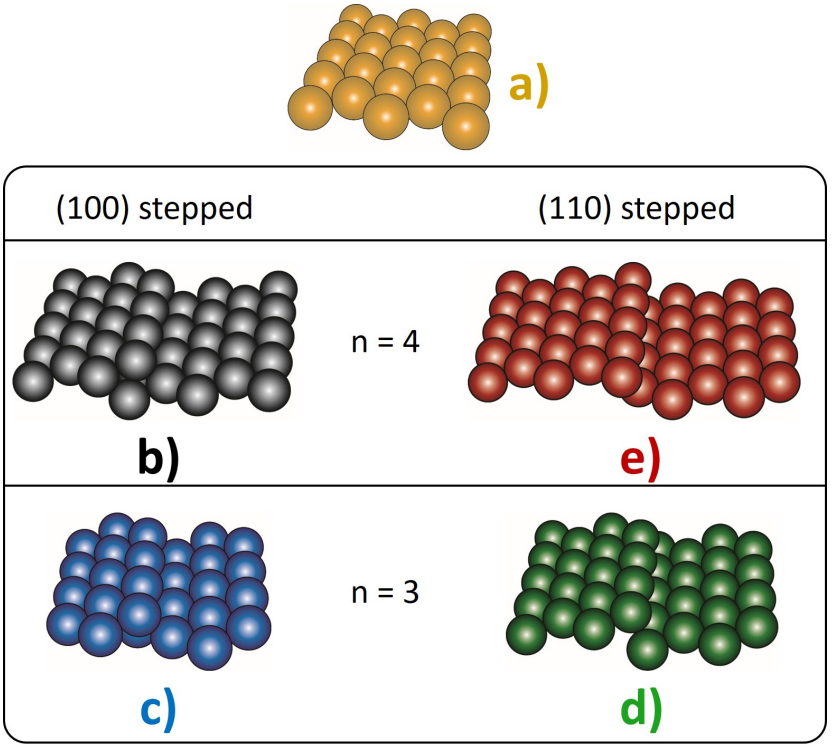

Figure 7.1: Schematic representation of a) Pt(111), b) Pt(533), c) Pt(211), d) Pt(221) and e) Pt(553). The LEED patterns are shown elsewhere [18, 19].

Figure 7.1 shows a schematic representation of Pt(111), Pt(533), Pt(221), Pt(553) and Pt(211) surfaces used in this study. Pt(211) and Pt(221) surfaces consist of three atom wide (111) terraces truncated with (100) and (110) step sites, respectively. Pt(533) and Pt(553) surfaces have four atom wide (111) terraces with (100) and (110) step geometries. Surfaces having 'n' atom wide (111) terraces with (110) step geometries can also be described as surfaces with 'n+1' atom wide (111) terraces truncated with (111) steps.

7.4 Results and discussion

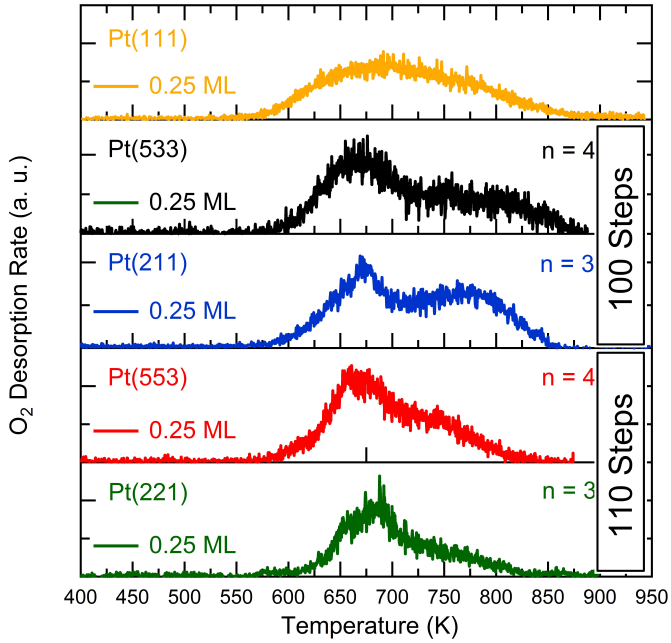

Figure 7.2: O_2 TPD spectra for Pt(111), Pt(211), Pt(221), Pt(553) and Pt(533) at 0.25 ML of recombinative oxygen coverage. n = terrace length of the (100) or (110) stepped surfaces.

Figure 7.2 shows TPD spectra for the recombinative desorption of O_2 from Pt(111), Pt(533), Pt(211), Pt(553), and Pt(221) after dosing with molecular oxygen at T_s = 100 K. The value of 'n' shown in Figure 7.2, indicates the terrace width of the Pt surfaces with (100) or (110) step geometries. As shown in previous work, O_2 desorption from Pt(111) occurs in a single, broad desorption peak[11, 14, 15, 35, 36, 39, 40] centered between 550 K and 750 K. This feature shows typical characteristics of second-order desorption kinetics. The maximum desorption rate for O_{ad} shifts to lower temperatures with increasing coverage and saturates at $\theta_{O_{ad}}$ = 0.25 ML. The TPD peak shape and the relative desorption kinetics are in good agreement with previous reports for Pt(111). Figure S2 in the supporting information quantitatively compares the uptake curve for Pt(111) to previous studies[11, 15].

On stepped surfaces, the broad desorption peak seen on Pt(111) separates into two desorption features. For both Pt(211) and (221), the lower temperature

feature is from recombinative desorption of O_{ad} from (111) terrace sites, whereas the higher temperature peak results from recombinative desorption from step sites [19–21, 41–43]. At $\theta_{O_{ad}} = 0.25$ ML, the peak desorption rate occurs at varying temperatures depending on step geometry. O_2 desorbs at a ~ 25 K lower temperature from (110) stepped surfaces than from (100) stepped surfaces, as reported previously[19]. The difference in desorption temperature was explained by density functional theory (DFT) calculations[44, 45] as arising from O atoms binding more strongly to (100) step sites than (110) step sites. Figure S1 in the supporting information provides additional information on the comparison and quantification of coverages for the various Pt surfaces.

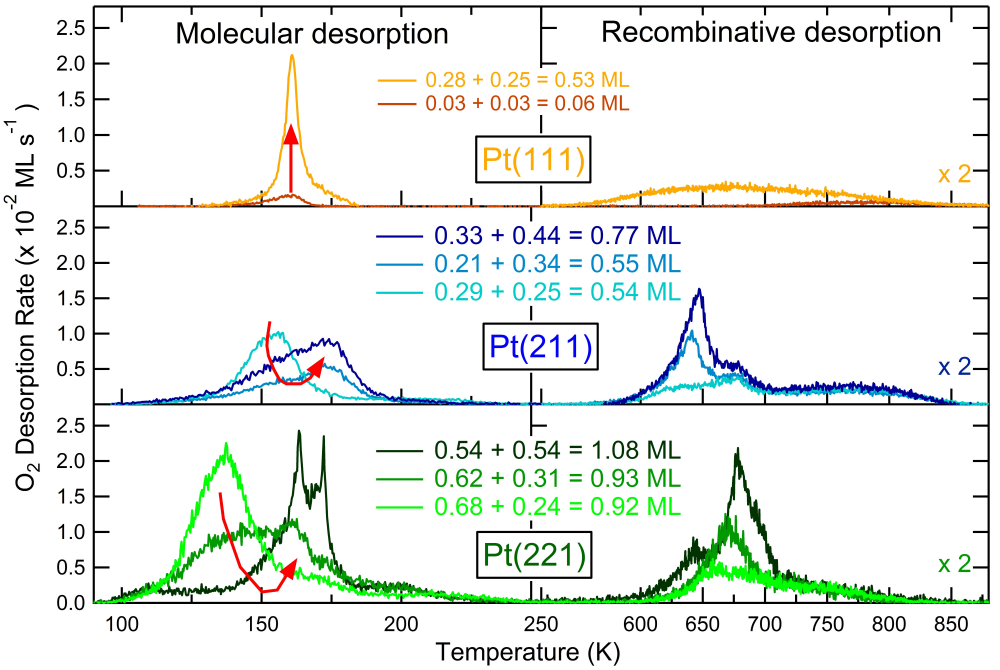

Figure 7.3: O_2 TPD spectra for a range of O_2 coverages obtained for O_2 doses at $T_s = 100$ K. The panels correspond to Pt(111) in the top panel, Pt(211) with (100) steps in the middle panel, and Pt(221) with (110) steps in the bottom panel.The left column shows desorption of molecularly adsorbed O_2, the right column shows recombinative desorption of O_{ad}.

O_2 dissociation at high temperature is not the only way oxygen can stick to Pt surfaces. At lower temperatures ($T_s < 150$ K), O_2 can molecularly adsorb as $O_{2,ad}$; an intact O_2 molecule chemisorbed to the surface. At low temperatures,

dissociatively chemisorbed O goes through an $O_{2,ad}$ precursor and both O_{ad} and $O_{2,ad}$ will be present on the surface. The total oxygen coverage (θ_O^{tot}) and the fraction of O_{ad} and $O_{2,ad}$ are strongly dependent on T_s[1, 8]. In order to thoroughly compare the O_2 adsorption behavior for the various crystal faces, TPD experiments were carried out in the $O_{2,ad}$ and O_{ad} temperature regimes; results are shown in figure 7.3. $O_{2,ad}$ desorbs from Pt(111) at 160 K, as seen in the top-left panel of figure 7.3, and O_{ad} atoms recombinatively desorb in the previously discussed broad, second-order desorption peak[19] (figure 7.2) shown in the top-right panel of figure 7.3. On Pt(111), exposures of up to 900 Langmuir (1 Langmuir = 10^{-6} Torr s^{-1}) O_2 demonstrate that $\theta_{O_{2,ad}}$ saturates at 0.28 ML, just slightly greater than the saturation coverage of 0.25 ML for O_{ad}, yielding θ_O^{tot} of 0.53 ML. We note that after extended O_2 exposures, the $O_{2,ad}$ desorption peak slightly shifted to a higher temperature, but the integrated intensity (total O) was unchanged. The total coverage of 0.53 ML is in good agreement with previous work done by Steininger et al., which, however, only explored O_2 exposures up to 40 Langmuir, so the desorption temperature shift was not observed[15].

The center panels of figure 7.3 show O_2 TPD data for Pt(211), 3-atom wide terraces with (100) steps, for three different θ_O^{tot}, 0.54 ML, 0.55 ML, and 0.77 ML. The partitioning between $\theta_{O_{ad}}$and $\theta_{O_{2,ad}}$ developed in an interesting fashion with increasing θ_O^{tot}. At θ_O^{tot} = 0.54 ML (figure 7.3, light blue), $O_{2,ad}$ desorbs in a single desorption peak at 155 K corresponding to $\theta_{O_{2,ad}}$= 0.29 ML (figure 7.3 center, left). The higher temperature TPD features (figure 7.3, center, right) arise from recombinative desorption of O_{ad}, and exhibit the saturation coverage of 0.25 ML discussed previously. With slightly larger exposure of O_2, the total O coverage modestly increased to 0.55 ML; however, the TPD features changed dramatically (figure 7.3, blue). At θ_O^{tot} = 0.55 ML, the intensity of the original $O_{2,ad}$ peak at 155 K diminished significantly, $\theta_{O_{2,ad}}$ decreased from 0.29 ML to 0.21 ML, and appears to split into two components; the original 155 K peak and a new peak at 174 K. The higher temperature desorption features also changed. The shoulder at 647 K develops into a sharp, well-defined peak while the higher temperature feature at 667 K did not increase with oxygen coverage. Likewise, the desorption of O_{ad} from steps between 700 K and 900 K was unchanged for all coverages discussed here. Continued exposure of Pt(211) to O_2 at T_s = 100 K saturated at θ_O^{tot} = 0.77 ML (figure 7.3, dark blue), and the TPD features were unaltered with additional O_2 exposure. At θ_O^{tot} = 0.77 ML, $\theta_{O_{2,ad}}$ increased to 0.33 ML and the shape of the desorption peak is similar to the peaks seen for θ_O^{tot} = 0.55 ML. Likewise, a monotonic increase in the higher temperature features is evident. The sharp peak at 647 K increased in intensity, and the other features remained the same. We have previously found that the stoichiometry and sharp desorption feature at 647 K

indicates formation of PtO lines on the (100) steps[18]. The general similarity that both Pt(111) and Pt(211) reach a saturation coverage suggest that dissociation of molecularly adsorbed oxygen only occurs during the temperature ramp. The sudden change in peak shape and distribution over molecular versus recombinative desorption around 0.55 ML indicates threshold behavior for dissociation. Above $\theta_{O_{ad}} = 0.25$ ML dissociation is enhanced during the temperature ramp at the expense of molecular desorption.

We now discuss O_2 desorption from Pt(221), which also has 3-atom wide terraces, like Pt(211), but the arrangement of the atoms along the step edges differ. Pt(221) has (110) step geometry instead of (100) as was the case for Pt(211). The lower panels in figure 7.3 show TPD data for O_2 desorption from Pt(221) with $\theta_O^{tot} = 0.92$ ML (light green), 0.93 ML (green), and 1.08 ML (dark green). It is worth noting that the oxygen coverages are significantly greater on Pt(221) than either Pt(211) or Pt(111). For θ_O^{tot} 0.92 ML and below, the TPD features uniformly increase in intensity with exposure. For $\theta_{O_{2,ad}}$ up to 0.68 ML, $O_{2,ad}$ desorbs in two desorption peaks, a larger one near 140 K and a shoulder at 163 K. The higher temperature O_{ad} recombinative desorption peak at $\theta_{O_{ad}} = 0.24$ ML is broad with a sharp feature around 650 K. Once $\theta_{O_{ad}}$ reached 0.24 ML, sticking of O_2 at Ts = 100 K formed $O_{2,ad}$. However, once θ_O^{tot} reached 0.92 ML, a dramatic change in the relative amounts of O_{ad} and $O_{2,ad}$ was observed. Recombinative desorption suddenly increases in size at the expense of molecular desorption. The sharp peak seen at 650 K intensifies and the peak temperature shifts upward towards 680 K. Additionally, a peak sharpens at 647 K. The molecular desorption regime also shows a concomitant shift toward higher desorption temperatures, and a new peak grows in at 173 K. For the highest coverage studied, $\theta_O^{tot} = 1.08$ ML, desorption is evenly split over the molecular and recombinative regimes with $\theta_{O_{2,ad}} = \theta_{O_{ad}} = 0.54$ ML. This behavior is in marked contrast to what was observed on Pt(211) with (100) step geometry, and planar Pt(111). Whereas both Pt(111) and (211) reached a terminal surface coverage with similar exposures, the continued evolution of $O_{2,ad}$ and O_{ad} desorption features indicates the Pt(221) surface is not saturated. Further details can be found in figure S2 in the supporting information.

The partitioning of oxygen into O_{ad} and$O_{2,ad}$ with respect to θ_O^{tot} is shown in figure 7.4 for Pt(111), Pt(211), Pt(553), and Pt(221). Pt(553) and Pt(221) have (110) step geometry and the step geometry is (100) on Pt(211). Figure 4 shows how the total amount of oxygen adsorbed during O_2 exposures at = 100 K desorbs either molecularly or recombinatively during TPD. All coverages are expressed with respect to the TPD integral for $\theta_{O_{ad}} = 0.25$ ML on Pt(111). Although the angular desorption characteristics vary for different desorption peaks on Pt(111)[46], these effects are not significant in our measurements and do not

interfere with directly comparing the relative coverages of the different surface species, as demonstrated in the Supporting Information. In each of the four plots in figure 7.4, the solid lines are local fits to data while dotted lines indicate critical oxygen coverages. The gray areas in figures 7.4a and 7.4b indicate the highest obtained oxygen coverage on Pt(111) and Pt(211) under background dosing conditions. It is clear that Pt(111) and Pt(211), with (100) step geometry, have substantially lower saturation coverages than Pt(211) and Pt(553) surfaces with (110) step geometry. Neither Pt(221) nor (553) showed evidence of saturation in our TPD experiments and the abscissa are the limits of total coverage probed in our experiments.

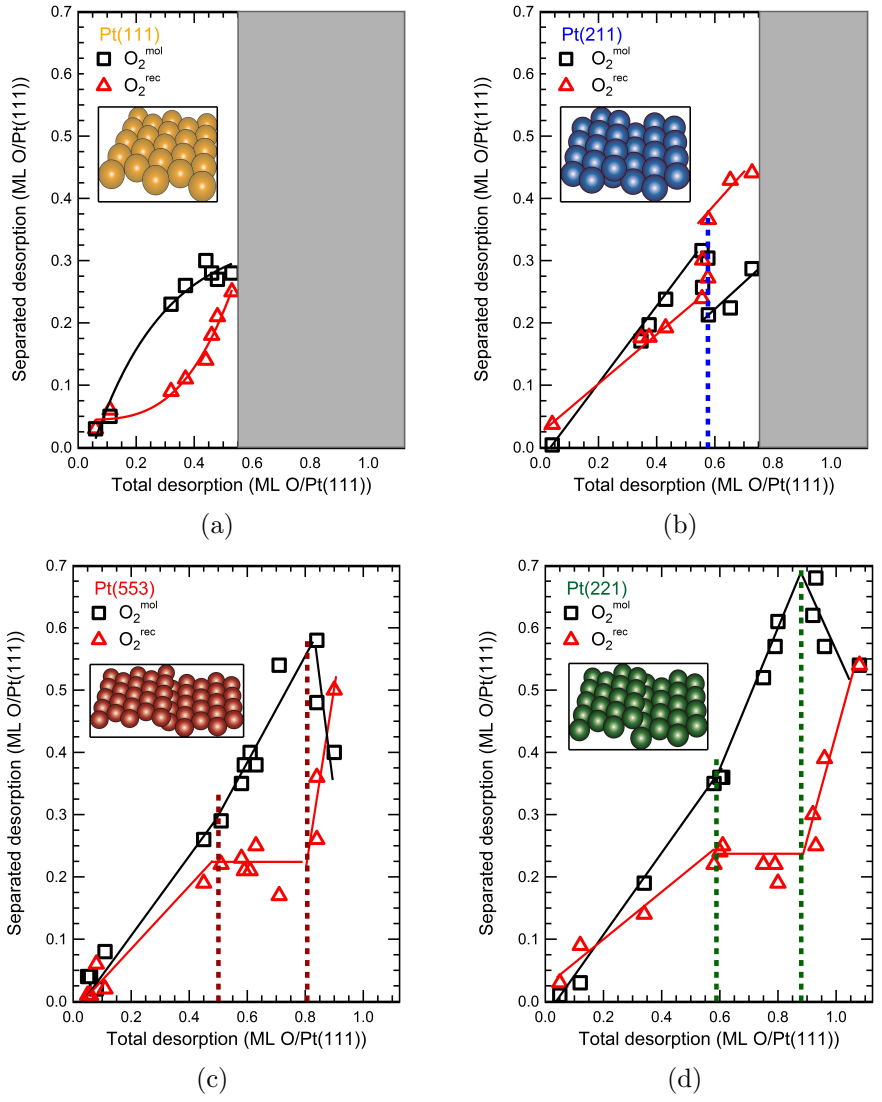

Figure 7.4: Integrated O_2 TPD signals for molecular and recombinative desorption as a function on initial O_2 coverage on a) Pt(111), b) Pt(211)[18], c) Pt(553) and d) Pt(221). The inset images show the surface representations and the solid lines are the fitted to the experimental data. The dotted lines emphasize the critical regions on the surfaces. The grey areas in figure 7.4a and figure 7.4b express the saturation coverage on Pt(111) and Pt(211).

We first consider the possible origins for the increase in O_2 uptake from planar

Pt(111) to the (100) stepped surfaces, which retain (111) atomic arrangements on the flat terraces. As discussed, O_2 adsorbs molecularly at 100 K on Pt(111), with a terminal $\theta_O^{tot} = 0.53$ ML. Dissociation only occurs during the temperature ramp, resulting in at most 0.25 ML O_{ad}, as shown by red triangles in figure 7.4a. It is important to note that dosing Pt(111) with O_2 at $T_s = 400$ K exclusively yields O_{ad} which saturates at $\theta_{O_{ad}} = 0.25$ ML. On Pt(211), saturation $\theta_{O_{ad}}$ is increased by 0.24 ML compared to Pt(111), representing a 45% increase in coverage. The number of Pt atoms per unit surface area is greater on corrugated Pt(211) than Pt(111). The ratio of geometric surface areas is 1.10, respectively, as described in detail in the Supporting Information. Now, if only $O_{2,ad}$ is packed on the Pt(211) surface at $T_s = 100$ K, then the packing density must be correspondingly higher on Pt(211) than on Pt(111), because of the increased surface area. This difference in geometric surface area accounts for, at most, 30% more $O_{2,ad}$ per unit area on Pt(211) than on Pt(111). Although attributing the increase in θ_O^{tot} exclusively to the changes in geometric surface is seemingly straightforward, it does not entirely account for the 45% increase observed. Low temperature dissociation of $O_{2,ad}$ could lead to the increase in θ_O^{tot}, but the differences are small enough that the observed uptake could be accounted for by the increased surface area.

Changes in the TPD spectra could indicate low temperature dissociation of $O_{2,ad}$. Lower $\theta_{O_{2,ad}}$ do not show any changes in the molecularly adsorbed O_2 TPD desorption features on Pt(211) (figure 7.3) up to $\theta_{O_{2,ad}} = 0.29$ ML. The absence of any changes in peak shapes suggests no coverage effects in the interactions between adsorbates. On Pt(211), the $O_{2,ad}$ molecular desorption peak is only 5 K lower than Pt(111), suggesting only small differences in the interadsorbate interactions. However, as θ_O^{tot} increases, the shifts in desorption features clearly shows changes in the interadsorbate interactions. For molecular desorption on Pt(211), the shift in intensity between the two desorption peaks, and the accompanying changes in the O_{ad} desorption features, point towards evolution in the nature of the surface. Although $\theta_{O_{2,ad}}$ does not increase very much, the $\theta_{O_{2,ad}}$ desorption peak shifts to 174 K. It is possible that these shifts are caused by the presence of atomic oxygen on the surface at low temperatures. As noted before, for Ts = 100 K O_2 exposures, dissociation of O_2 occurs during the TPD ramp, and above the $O_{2,ad}$ desorption temperature. Therefore, in order for O_{ad} to alter the interadsorbate interactions, it must dissociate at much lower temperatures than occurring for thermally induced dissociation on Pt(111). Although some dissociation may have occurred at the dosing temperature or early on in the ramp as a consequence of the combined presence of the (100) steps and a densely packed initial O_2 overlayer, we do not find that the changes on desorption peak temperature or θ_O^{tot} in our data to be particularly convincing to argue for or against dissociation at 100 K.

Alternatively, for the surfaces with (110) step geometry, the changes in the TPD spectra strongly indicate dissociative adsorption at 100 K. As shown in figure 7.4d, the changes in oxygen uptake on Pt(221) are far more pronounced. Not only does the desorption shift from single peak at 140 K to two peaks at 164 K and 173 K, but θ_O^{tot} increases by at least $\theta_O^{tot} = 0.50$ ML, an 85% increase from Pt(111). A similar increase is observed for Pt(553), shown in figure 7.4c. The increased number of adsorption sites because of the larger geometric surface area, while close for Pt(211), is far from sufficient to account for the increase in θ_O^{tot} on Pt(221). Pt(221) has a 16% larger geometric surface area that Pt(111), so in order to account for the 85% increase in oxygen coverage, a 60% increase in packing density of $O_{2,ad}$ would be required. This is not a plausible expectation because the majority of the surface is still regular (111) terraces. Formation of a second layer of $O_{2,ad}$ at 100 K is not supported by the TPD data; an overlayer would exhibit a significantly decreased desorption temperature[47, 48], which was not observed. As increases in geometric surface area, packing density, or overlayers are not adequate to account for the excess oxygen adsorption observed, low temperature dissociation of O_2 on (110) steps must be considered. Dissociation of $O_{2,ad}$ results in an overlayer consisting of $O_{2,ad}$ and O_{ad} covering the terraces and steps of the surface. This conclusion is supported by significant changes in the predominant $O_{2,ad}$ desorption peak. At $\theta_{O_{2,ad}} = 0.68$ ML, the peak desorption temperature is 20 K lower than on Pt(111); the temperature difference was only ≈ 5 K on Pt(211). A Redhead analysis of the larger difference for Pt(221) suggests a drop in desorption energy from the molecular state of 7.0 kJ mol^{-1}, when assuming a prefactor of 1x10^{-13} s^{-1}. Both Pt(221) and Pt(553) surfaces display similar O uptakes and distributions between molecular and recombinative desorption, suggesting the narrow step widths on Pt(221) are not the cause of the enhanced uptake. As the marked change in O uptake is more prominent going from Pt(211) to Pt(221), with similar step-widths and abundance of (111) terraces, it is the (110) step geometry that dissociates $O_{2,ad}$ and causes the increase in O uptake.

With the (110) surfaces inducing $O_{2,ad}$ dissociation at moderate to high coverages established, we now consider whether dissociation occurs for low θ_O^{tot}, i.e. along the initial increase in figure 7.4c and 7.4d. The plateau in both traces at $\theta_{O_{ad}} \approx 0.25$ ML supports the notion that this is indeed the case. For the lowest θ_O^{tot}, O_2 adsorption is evenly split between O_{ad} and $O_{2,ad}$. After this initial period of rapid O_2 dissociation, dissociation is self-limited to a maximum of 0.25 ML O/Pt. For θ_O^{tot} greater than ≈ 0.6 ML on Pt(221), or 0.5 ML for Pt(553), recombinative desorption plateaus while molecular desorption increases linearly for either surface. This suggests that the adsorption energy (E_{ads}) is independent of $\theta_{O_{2,ad}}$ in this coverage regime, and the chemical species present and surface

structures are invariant. However, we are unable to unambiguously attribute the increase in coverage to low-temperature $O_{2,ad}$ dissociation from the TPD results alone, because this argument holds true if dissociation for smaller initial coverages occurs between 100 K and 140 K. To resolve this issue, we must determine if O_{ad} is present on a Pt surface with (110) step geometry at 100 K.

The threshold behavior is the last point we wish to address regarding figure 7.4. Sudden additional dissociation at the expense of desorption occurs for both (110) and (100) stepped surfaces at $\theta_{O_{ad}} = 0.25$ ML. For both step types, the increase in dissociative adsorption is associated with an increase in the desorption temperature of $O_{2,ad}$ as well as the appearance of sharp desorption peaks in the recombinative desorption regime. The latter have been connected to formation of PtO_2 along the (110) steps, as shown in previous work on Pt(111)[13]. The formation of PtO_2 is also supported by the overlapping leading edges of the TPD features, which is characteristic of a phase transition. As O_2 has also been shown to bind more strongly on the metal oxide than the metal surface[22], we interpret the thresholds as the minimal $\theta_{O_{ad}}$ required for additional oxidation of the Pt surface, i.e. dissociation beyond regular dissociative adsorption on (111) terrace sites and step edges. Stabilizing interactions between $O_{2,ad}$ and the previously formed O_{ad} phase causes the temperature upshift for the molecular desorption feature occurring at the higher exposures. The increased binding leads to additional dissociation and formation of local metal oxides that decompose in the sharp desorption features in the recombinative regime, further supporting the formation of PtO_2. As previously argued for the (100) stepped surface, our data does not require the initial dissociation to occur at 100 K. However, dissociation must happen at all initial coverages somewhere between 100 K and 150 K. If it does not happen at 100 K, or at most to a small extent for the highest exposure, the limited total uptake for (211) makes sense. Most dissociation only occurs during the temperature ramp, leading to significant loss of O_2 through parallel molecular desorption and prior to the onset of local surface metal oxide formation. As initial dissociation is better facilitated by the (110) step at 100 K, more O_2 binds at a lower temperature, in part as a 0.25 ML O_{ad}. With a minimal additional concentration of $O_{2,ad}$ that spans the plateau, molecular adsorption locations and/or geometries are present that facilitate local formation of a surface metal oxide.

Our TPD results clearly indicate that O_2 dissociation depends strongly on the step geometry at low temperatures. In the supporting information, we present an alternate means to support this point. Whereas we could not conclude this with any certainty for Pt(211), both (110) stepped surfaces dissociate molecular oxygen, at least for higher coverages, at 100 K. For lower initial coverages, we

could not argue this based on TPD results, although the coverage-dependencies seem to suggest it. In order to resolve this we have taken images of the Pt(553) surface using STM in the Chicago laboratory.

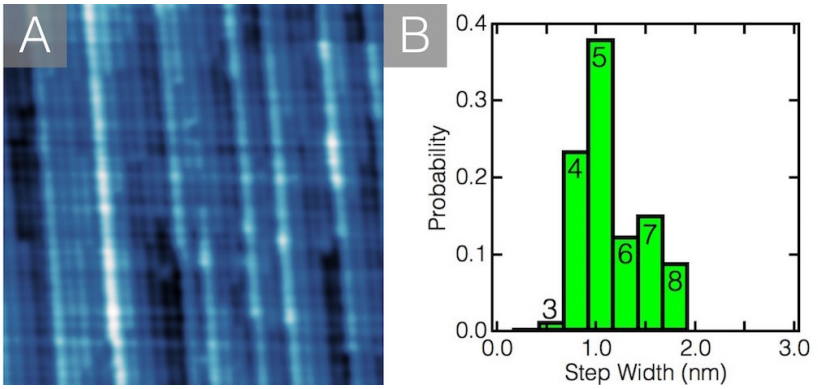

Figure 7.5: The left panel (A) shows an STM image of the clean Pt(553), T_{STM} = 30 K, V = 1.0 V, I = 250 pA, 40 nm x 40 nm. The statistical analysis of the step width Pt(553) leads to the histogram shown in the right panel (B).

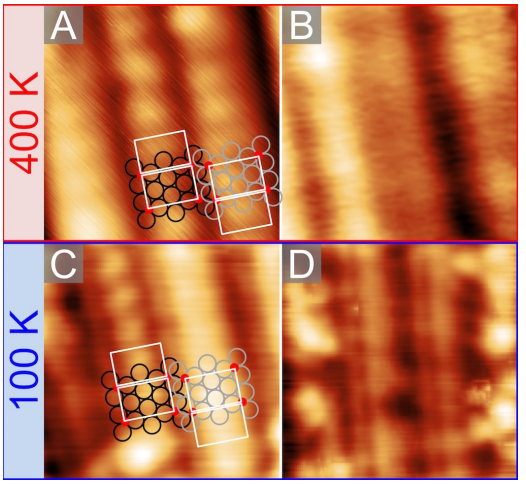

Figure 7.6: 4nm x 4 nm STM images of oxygen covered Pt(553) taken at T_{STM} = 30 K. A) 3 L O_2 exposure at 400 K, V = 0.92 V, I = 160 pA, B) 0.6 L O_2 exposure at 400 K, V = 0.70 V, I = 150 pA, C) 2 L O_2 exposure at 100 K, V = 0.15 V, I = 90 pA, D) 0.6 L O_2 exposure at 100 K, V = 0.78 V, I = 190 pA.

In order to obtain a reliable standard for the structure of Pt(553), we first

imaged the clean Pt(553) surface. A typical image is shown figure 7.5A. Due to surface relaxation and slight misalignment during the crystal preparation process, the surface is not uniformly comprised of five atom wide (111) terraces separated by monotonic steps. While the LEED pattern corresponding to Pt(553) has a spot-splitting to row-spacing ratio that indicates an average terrace width of five atoms, describing this surface as Pt[5(111)x(111)] which is equivalent to Pt[4(111)x(110)], the sub-nanometer scale resolution of STM shown in figure 7.5A allows us to determine the actual distribution of terraces widths. Figure 5B shows this distribution of terrace widths in the form of a histogram. Over 60% of the steps are either 5 or 4 atoms wide with the 5-atom wide terraces being the most abundant. This distribution of terrace widths allows us to study O adsorption on a (110) step type surface with known terrace variances; knowing that there is a distribution of terrace widths allows us to relate adsorption behavior to step type rather than terrace width. It is also important to note the variance in contrast across the clean metal surface. As has been shown when imaging other stepped metal surfaces, the high corrugation of the surface, coupled with inherent imaging limitations, causes steps to display with varying contrast in the STM image[38, 49, 50].

O_{ad} is the only oxygen species after O_2 exposure at 400 K, so the Pt(553) crystal was exposed to 3 L of O_2 at Ts = 400 K to provide a reference image for $\theta_{O_{ad}} = 0.25$ ML and no $O_{2,ad}$. After exposure, the sample was transferred to the STM and cooled to 30 K for imaging. Figure 7.6A shows an image of the oxidized surface along with an illustration of the positions of oxygen and Pt atoms. The oblong rectangular features present in figure 7.6A are highlighted with a white rectangle and correspond to four oxygen atoms resting in fcc tetragonal hollow sites; the arrangement of oxygen on Pt(553) has been determined by previous work[44]. As molecularly adsorbed oxygen is not stable at the 400 K exposure temperature[8], the oblong features must result from the presence of O_{ad}. As seen in figure 7.6A, each of the three terraces imaged possess the rectangular features. The terrace on the left hand side is slightly wider than the two remaining terraces. Despite the difference in terrace width, the appearance of the step in the image is the same. The step terrace has the same rectangular feature characteristic of four O_{ad} on a (111) terrace. We also imaged the surface after exposure to 0.6 L O_2 at $T_s = 400$ K to determine if the surface structure is coverage dependent. As shown in figure 7.6B, the surface is now mostly clean terraces with bright features aligning along the step edges instead of the rectangular features spanning the steps. The orientation of the images is such that the steps move downward from right to left across all four images. The location of the bright oxygen features along the edge of the step, with a slight dark region behind the bright feature,

suggests that the oxygen is also aligning in the tetragonal hollows of the fcc surface at low coverages.

We now look at the Pt(553) surface after low temperature exposures to O_2 to determine if the features characteristic of O_{ad} are present, indicating low temperature dissociation of $O_{2,ad}$ on (110) stepped surfaces. The Pt(553) surface was exposed to 2 L O_2 ($\theta_O^{tot} \approx 0.7$ ML) at $T_s = 100$ K, and the STM images are shown in figure 7.6C. At this temperature, T_s is too low to activate dissociation, and $O_{2,ad}$ is most stable on (111) terraces[8]. If $O_{2,ad}$ does not, in fact, dissociate, we would not expect to see the surface uniformly covered by the rectangular features identified in figure 7.6A. This is clearly not the case. As shown in figure 7.6C, the Pt(553) surface after $T_s = 100$ K exposure to O_2 is very similar to the surface after 400 K O_2 exposure. This suggests that $O_{2,ad}$ dissociated, forming O_{ad} on the terraces. This is shown in figure 7.6C as the presence of rectangular features along the center-left terrace while the center-right terrace appears to be covered in uniformly bright adsorbates. Post-imaging TPD of the sample confirms that no appreciable accumulation of contaminants occurs during imaging, so the bright, rectangular features must be O_{ad}. The coexistence of O_{ad} and $O_{2,ad}$ accurately represents TPD data which indicates the presence of both oxygen species. Because the sample was exposed to O_2 at 100 K, below the temperature needed for dissociation of oxygen on Pt(553), the oxygen must dissociate upon adsorption to the surface. This cannot be because of the direct channel for dissociation, because the translational energy of the incident O_2 is insufficient to activate dissociation[8]. To check for coverage effects, the Pt(553) surface was also exposed to 0.6 L ($\theta_O^{tot} \approx$ 0.2 ML) at 100 K. A representative STM image is shown in figure 7.6D. Although the exposure is the same as for the image in figure 7.6B, the structures along the terraces after the 100 K exposure well-resolved. Rather than oblong rectangular features, a striped pattern near the step edge presents itself. The orientation of the dark contrast in figure 7.6D corresponds well to the dark contrast near the bright feature along the step edge in figure 7.6B. The presence of similar structural features for 0.6 L O_2 exposure at 100 K and 400 K shows that O_2 dissociation occurs at 100 K even for very low O_2 coverages. Finally, the actual terrace widths on the Pt(553) crystal are not uniform (see figure 7.5B), so it can be determined that the dissociation observed at low temperatures on Pt(553) is due to the (110) step geometry rather than the terrace width. The STM images clearly support the findings from the TPD experiments. This demonstrates that the height of dissociation barriers is sensitive to step geometry.

Summarizing, (100) stepped Pt surfaces exhibit high reactivity at lower oxygen coverages (≈ 0.6 ML), however, the reactivity decreases with increasing coverage. On the other hand, (110) stepped Pt surfaces require more oxygen to achieve the

high reactivity but they maintain the high reactivity up to higher coverages (> 0.8 ML). Additionally, extended O_2 exposures saturated the (100) stepped surfaces whereas on the (110) steps, no such saturation was observed.

7.5 Conclusion

Our results show low-temperature dissociation of O_2 on Pt surfaces is strongly dependent on the arrangement of Pt atoms on monoatomic steps. This demonstrates the complexities of O_2 adsorption behavior that arise when defect sites are accounted for on catalytically active surfaces. A combination of TPD and STM experiments show that (100) and (110) step types have very different adsorption and desorption behaviors. Although surfaces with (100) steps show an increase in oxygen coverage compared to Pt(111), this can be attributed to the increased areal density of Pt atoms on the corrugated surfaces. However, on surfaces with (110) step geometries, this increase in surface area cannot account for the increased oxygen coverage. STM images after exposures of Pt(553) to O_2 at $T_s = 400$ K or 100 K clearly show similar surface structures. Only O_{ad} can be on the surface after $T_s = 400$ K O_2 exposures; because the surface structures are similar, O_{ad} must also be present after $T_s = 100$ K O_2 exposures. Therefore, O_2 dissociates upon adsorption on surfaces with (110) steps and not only during the TPD ramp. The presence of O_{ad} confirms that O_2 dissociation at low temperatures causes the increased oxygen uptake. This demonstrates that step geometry is the determining factor in low temperature O_2 dissociation. The (110) steps must lower the dissociation barrier in ways steps with (100) geometry cannot.

7.6 Bibliography

References

(1) Zambelli, T; Barth, J. V.; Wintterlin, J; Ertl, G *Nature* **1997**, *390*, 495–497.

(2) Bonn, M. *Science* **1999**, *285*, 1042–1045.

(3) Sutter, E. a.; Tong, X.; Jungjohann, K.; Sutter, P. W. *Proceedings of the National Academy of Sciences of the United States of America* **2013**, *110*, 10519–24.

(4) Gustafson, J.; Mikkelsen, A; Borg, M.; Andersen, J.; Lundgren, E.; Klein, C.; Hofer, W.; Schmid, M.; Varga, P.; Köhler, L.; Kresse, G.; Kasper, N.; Stierle, A.; Dosch, H. *Physical Review B* **2005**, *71*, 115442.

(5) Wintterlin, J. *Science* **1997**, *278*, 1931–1934.

(6) Hawkins, J. M.; Weaver, J. F.; Asthagiri, A. *Physical Review B* **2009**, *79*, 125434.

(7) Bradley Shumbera, R.; Kan, H. H.; Weaver, J. F. *Surface Science* **2007**, *601*, 4809–4816.

(8) Luntz, A. C.; Williams, M. D.; Bethune, D. S. *Journal of Chemical Physics* **1988**, *89*, 4381–4396.

(9) Nolan, P.; Lutz, B.; Tanaka, P.; Davis, J.; Mullins, C. *The Journal of chemical physics* **1999**, *111*, 3696–3704.

(10) Stipe, B.; Rezaei, M.; Ho, W; Gao, S; Persson, M; Lundqvist, B. *Physical review letters* **1997**, *78*, 4410.

(11) Winkler, A.; Guo, X.; Siddiqui, H. R.; Hagans, P.; Yates, J. T. *Surface Science* **1988**, *201*, 419–443.

(12) Wang, H; Tobin, R. G.; Lambert, D. K.; DiMaggio, C. L.; Fisher, G. B. *Surface Science* **1997**, *372*, 267–278.

(13) Devarajan, S. P.; Hinojosa Jr., J. A.; Weaver, J. F. *Surface Science* **2008**, *602*, 3116–3124.

(14) Gland, J. L.; Sexton, B. A.; Fisher, G. B. *Surface Science* **1980**, *95*, 587–602.

(15) Steininger, H; Lehwald, S; Ibach, H *Surface Science* **1982**, *123*, 1–17.

(16) Weaver, J. F.; Chen, J. J.; Gerrard, A. L. *Surface Science* **2005**, *592*, 83–103.

(17) Weaver, J. F.; Kan, H. H.; Shumbera, R. B. *Journal of Physics-Condensed Matter* **2008**, *20*.

(18) Badan, C.; Koper, M. T. M.; Juurlink, L. B. F. *The Journal of Physical Chemistry C* **2015**, *119*, 13551–13560.

(19) Van der Niet, M. J. T. C.; den Dunnen, A.; Juurlink, L. B. F.; Koper, M. T. M. *Journal of Chemical Physics* **2010**, *132*, 174705–174713.

(20) Van der Niet, M. J. T. C.; den Dunnen, A.; Juurlink, L. B. F.; Koper, M. T. M. *Physical Chemistry Chemical Physics* **2011**, *13*, 1629–1638.

(21) Van der Niet, M. J. T. C.; den Dunnen, A.; Juurlink, L. B. F.; Koper, M. T. M. *Angewandte Chemie-International Edition* **2010**, *49*, 6572–6575.

(22) Wang, J. G.; Li, W. X.; Borg, M.; Gustafson, J.; Mikkelsen, a.; Pedersen, T. M.; Lundgren, E.; Weissenrieder, J.; Klikovits, J.; Schmid, M.; Hammer, B.; Andersen, J. N. *Physical Review Letters* **2005**, *95*, 1–4.

(23) Parker, D. H.; Bartram, M. E.; Koel, B. E. *Surface Science* **1989**, *217*, 489–510.

(24) Saliba, N.; Tsai, Y.-L; Panja, C; Koel, B. *Surface Science* **1999**, *419*, 79–88.

(25) Ohno, Y.; Matsushima, T. *Surface Science* **1991**, *241*, 47–53.

(26) Zhu, T.; Sun, S.-G.; van Santen, R. A.; Hensen, E. J. *The Journal of Physical Chemistry C* **2013**, *117*, 11251–11257.

(27) Li, W.; Österlund, L.; Vestergaard, E.; Vang, R.; Matthiesen, J; Pedersen, T.; Lægsgaard, E.; Hammer, B; Besenbacher, F *Physical Review Letters* **2004**, *93*, 146104.

(28) Walker, A.; Klötzer, B; King, D. *The Journal of chemical physics* **1998**, *109*, 6879–6888.

(29) Gambardella, P; Sljivancanin, Z; Hammer, B; Blanc, M; Kuhnke, K; Kern, K *Physical Review Letters* **2001**, *87*.

(30) Kratzer, P.; Pehlke, E.; Scheffler, M.; Raschke, M. B.; Hofer, U. **1998**, 5.

(31) Šljivan, Ž.; Hammer, B. *Physical Review B* **2010**, 1–4.

(32) Badan, C.; Heyrich, Y.; Koper, M. T. M.; Juurlink, L. B. F. *The Journal of Physical Chemistry Letters* **2016**, 1682–1685.

(33) Vanhove, M. A.; Somorjai, G. A. *Surface Science* **1980**, *92*, 489–518.

(34) Henzler, M *Surface Science* **1970**, *19*, 159–171.

(35) Puglia, C.; Nilsson, a.; Hernnäs, B.; Karis, O.; Bennich, P.; Mårtensson, N. *Surface Science* **1995**, *342*, 119–133.

(36) Norton, P.; Davies, J.; Jackman, T. *Surface Science* **1982**, *122*, L593–L600.

(37) Derouin, J.; Farber, R. G.; Killelea, D. R. *Journal of Physical Chemistry C* **2015**, *119*, 14748–14755.

(38) Kolb, M. J.; Farber, R. G.; Derouin, J.; Badan, C.; Calle-Vallejo, F.; Juurlink, L. B. F.; Killelea, D. R.; Koper, M. T. M. *Physical Review Letters* **2016**, *116*, 136101.

(39) Bashlakov, D.; Juurlink, L.; Koper, M.; Yanson, A. *Catalysis Letters* **2012**, *142*, 1–6.

(40) Avery, N. R. *Chemical Physics Letters* **1983**, *96*, 371–373.

(41) Rar, A.; Matsushima, T. *Surface Science* **1994**, *318*, 89–96.

(42) Gee, A. T.; Hayden, B. E. *The Journal of Chemical Physics* **2000**, *113*, 10333–10343.

(43) Ogawa, T.; Kuwabara, A.; Fisher, C. A. J.; Moriwake, H.; Miwa, T. *Journal of Physical Chemistry C* **2013**, *117*, 9772–9778.

(44) Kolb, M. J.; Calle-Vallejo, F.; Juurlink, L. B. F.; Koper, M. T. M. *The Journal of chemical physics* **2014**, *140*, 134708.

(45) Feibelman, P.; Esch, S.; Michely, T. *Physical Review Letters* **1996**, *77*, 2257–2260.

(46) Allers, K.-H.; Pfnür, H; Feulner, P; Menzel, D *Zeitschrift für Physikalische Chemie* **1996**, *197*, 253–268.

(47) Gibson, K.; Sibener, S.; Hall, B. M.; Mills, D.; Black, J. *The Journal of Chemical Physics* **1985**, *83*, 4256–4270.

(48) Kimmel, G. A.; Persson, M.; Dohnalek, Z.; Kay, B. D. *The Journal of Chemical Physics* **2003**, *119*, 6776–6783.

(49) Ding, H.; Stepanyuk, V.; Ignatiev, P.; Negulyaev, N.; Niebergall, L; Wasniowska, M; Gao, C.; Bruno, P; Kirschner, J *Physical Review B* **2007**, *76*, 033409.

(50) Pearl, T.; Sibener, S. *The Journal of Physical Chemistry B* **2001**, *105*, 6300–6306.